River dissolved inorganic carbon losses from the Andes to lowland Amazon via cryptic sedimentary exchange processes

Robert G. Hilton[1,2,*], A. Joshua West[3], Mark H. Garnett[4], Kirsty Harrington[5], Victoria Alcock[2], Mathieu Dellinger[6], Emily Burt[3,8], Adan Julian Ccahuana Quispe[7], Philippa Ascough[4], Joshua F. Dean[9], Yinxue Liu[1]

[1]School of Geography and the Environment, University of Oxford, Oxford, UK

[2]Department of Earth Sciences, University of Oxford, Oxford, UK

[3]Department of Earth Sciences, University of Southern California, Los Angeles, California 90089, USA

[4]NEIF Radiocarbon Laboratory, SUERC, East Kilbride, UK

[5]Smith School of Enterprise and the Environment, University of Oxford, UK

[6]Environnements DYnamiques et TErritoires de la Montagne (EDYTEM), CNRS - Université Savoie Mont-Blanc, 73370 Le Bourget-Du-Lac, France

[7]Escuela Profesional de Biologia, Facultad de Ciencas, Universidad Nacional de San Antonio Abad del Cusco, Cusco 08000, Peru

[8]Department of Natural Resources and Environmental Sciences, University of Nevada, Reno, USA

[9]School of Geographical Sciences, University of Bristol, Bristol, UK

*corresponding author: robert.hilton@ouce.ox.ac.uk

Abstract

River carbon transfers and associated greenhouse gas emissions are a major component of the carbon cycle. Proposals to use rivers and their catchments to increase carbon dioxide (CO_2) drawdown, by enhanced rock weathering and river alkalinity enhancement, require secure delivery of dissolved inorganic carbon (DIC) and increased cation loads (e.g. Ca^{2+}) to the ocean. Here we explore the fate of river DIC across hundreds of kilometres on an Andes to Amazon floodplain transect, where natural weathering fluxes are high. The holistic transfer of dissolved cations, DIC and CO_2 release were determined, alongside radiocarbon-based insight on carbon source, in two seasonal campaigns in 2019. In the wet season, river CO_2 release was high and sustained: equivalent to 30-100 % of the instantaneous river DIC flux. A reach-scale weathering budget showed ancient DIC from carbonate minerals mixing with decadal-aged CO_2. Across the river reach during the wet season, instantaneous fluxes

revealed that 21 ± 6 % of DIC and 13 ± 7 % of Ca^{2+} were lost across the lowland floodplain from upstream to downstream. These losses are attributed to a set of inorganic processes dominated by cation exchange, alongside a potential role for addition of other weathering acids and secondary carbonate formation. Not often considered in models of river DIC export, these cryptic sedimentary processes could reduce the CO_2 drawdown efficiency achieved by carbon cycle management of river geochemistry by 10s of percent or more, particularly in catchments where sediment loads have been perturbed by human activities.

Significance statement

Technologies are needed to remove carbon dioxide from the atmosphere to help stop the worst impacts of climate change. There are proposals that use rivers to help remove carbon dioxide from the atmosphere, but these only work if they can carry carbon produced by rock weathering to the ocean. Using geochemical, flux, and radiocarbon measurements along an Andes–Amazon floodplain transect, we quantify the fate of dissolved inorganic carbon and weathering-derived cations during downstream transport. We find substantial wet-season CO_2 evasion and significant floodplain losses of both DIC and Ca^{2+}. Mass balance and isotopic evidence indicate that inorganic sedimental processes, particularly cation exchange, drive geochemical reactions that create CO2 gas, which can easily be released into the atmosphere. These processes are not routinely represented in river carbon export models but may reduce effective carbon sequestration efficiencies associated with enhanced weathering and river alkalinity enhancement by tens of percent.

Introduction

Rivers play a central role in the carbon cycle, acting to exchange carbon between the atmosphere, biosphere and lithosphere[1–3]. As such, processes in river catchments impact Earth's climate across a range of timescales[4,5], with modern-day river surfaces acting as a net source of 2.0 (1.6-2.2) PgC yr^{-1} of carbon dioxide (CO_2) alongside other greenhouse gases (e.g. methane) to the atmosphere[2,6,7]. Rivers also carry carbon in dissolved and particulate form which can contribute to the generation of these greenhouse gas emissions[8–10] or act as a longer-term sink through storage in the ocean and/or accumulation in continental and marine sediments[11–13]. A key component that connects river carbon pools is dissolved inorganic carbon (DIC, the sum of dissolved carbon species, CO_2, HCO_3^- and CO_3^{2-}), which is controlled by chemical weathering across terrestrial landscapes[3], alongside the biogeochemical processes that form and consume organic matter (OM)[14,15]. Understanding the river DIC pool is thus critical to assessing both river CO_2 emissions that play out in the contemporary carbon

cycle[2,16–18], and the export of DIC and associated dissolved cations to the oceans that stores carbon over >10^3 year timescales[19].

River DIC export could be increased through Enhanced Rock Weathering (ERW), as a proposed carbon cycle management solution to reach net zero emissions[20–22]. In addition, direct increases in river DIC are also being considered via River Alkalinity Enhancement (RAE) projects[23]. Both methods rely on the increased supply of cations (e.g. Ca^{2+}, Mg^{2+}) through the chemical weathering of silicate minerals[21] and carbonate minerals[24] for ERW, or through direct inputs to rivers for RAE. Field trials are underway for ERW that suggest that fine basalt powder additions to agricultural fields can undergo dissolution on annual timescales[25]. For these CO_2 removal processes to be effective, the newly produced weathering products (Ca^{2+}, Mg^{2+}) and associated DIC need to reach the oceans where the storage of DIC is stable over thousands of years[26]. Current carbon credit markets rely on protocols[23] that still retain large uncertainties in the transport of carbon through rivers[27,28].

River CO_2 emissions represent a potential net loss of the river DIC pool and could impact the net CO_2 drawdown that arises from any modifications to river chemistry from ERW or RAE[28]. For instance, river CO_2 release could act to increase pH and the saturation state of calcium carbonate, which could be a sink of Ca^{2+} and DIC. Modelling scenarios suggest secondary calcite precipitation in river systems could lower the efficiency of ERW CO_2 removal by 16-27% [29]. In addition, the pre-existing dissolved chemistry of a river places an upper bound on any potential CO_2 drawdown, set by river CO_2 release and carbonate precipitation[24,30]. Loss of ERW and RAE -derived cations and DIC could also occur through cation exchange reactions on sedimentary grains[31]. Analogous to processes identified as important in soils and shallow groundwaters[32], the exchange of dissolved Ca^{2+} with H^+ ions could reduce the DIC pool if this forces CO_2 degassing, and/or lead to a delayed impact of ERW on stream and river geochemistry and resulting CO_2 drawdown. Finally, inputs of acidity from natural and anthropogenically modified sources could drive DIC loss. Losses could be driven by increasing sulfide oxidation in permafrost and mountain environments[33,34], mining impacts on sulfuric acid generation[35] and nitric acids from fertilisers[36].

While models suggest river CO_2 release could impact the security of DIC export to the ocean and thus ERW and RAE outcomes[24,29], we lack field measurements to understand and quantify key processes and assess baseline drivers of net DIC loss in rivers. One challenge is that the net heterotrophy of many river systems, where OM respiration within and around river channels fuels high dissolved CO_2 concentrations[9,37], means that high river CO_2 emissions may not necessarily reflect a net reduction of river DIC export. In addition, while net annual river CO_2 emissions and fluxes are generally well constrained at the global scale[2,6], many estimates are derived from indirect estimates of dissolved CO_2 concentration (from pH,

104 temperature, and alkalinity) and/or indirect measurements of CO_2 emissions (from CO_2
105 concentration and gas exchange velocity). Finally, catchment-scale measurements of
106 weathering pathways and fluxes[38] are not often linked to assessment of river CO_2 source[18].
107 To move forward, we need to i:) quantify CO_2 losses in the context of the exported river DIC
108 flux; ii) assess weathering inputs and the role of carbonate and silicate mineral weathering as
109 sources of DIC; iii) consider the role of strong acids (sulfuric acid, nitric acid) in the dissolved
110 geochemistry; iv) track river sediment geochemistry to assess water-sediment interactions
111 and secondary carbonate formation.

112 Here we provide new insight on the intertwined fates of river DIC and CO_2 and their
113 link to weathering inputs and secondary inorganic processes. We use hydrochemical methods
114 to quantify water, DIC and solute fluxes during field campaigns in the wet and dry seasons
115 (March and May 2019) over hundreds of kilometres of an Andes mountains to Amazon
116 foreland floodplain transect (Fig. 1A) with high geochemical weathering rates [39,40]. We combine
117 the quantification of weathering inputs with radiocarbon and stable isotope measurements of
118 river CO_2, DIC, particulate organic carbon (POC) and particulate inorganic carbon (PIC), to
119 track carbon sources. We find sustained CO_2 release across the transect is driven by OM
120 respiration that is older than previously noted in other tropical rivers. The measurements reveal
121 a net river DIC and Ca^{2+} loss downstream in the wet season, which we assess considering
122 additional weathering pathways and secondary processes associated with river sediments.
123 Our findings suggest natural river systems have unseen complexities that will impact the fate
124 of ERW and RAE applications, challenge assumptions regarding the security of river DIC
125 export and effectiveness of CO_2 drawdown.

126

127 **RESULTS**

128 **Sustained river CO_2 release from the Andes to Amazon floodplain**

129 The rates of river CO_2 release across the sampling transect were high in the wet season
130 (Methods, Table S1), ranging from 2.77 – 19.9 μmol m^{-2} s^{-1}, an average of 7.4 ± 2.9 μmol m^{-2}
131 s^{-1} (n = 12, ± 2 standard error unless otherwise stated). These measurements are similar to
132 river CO_2 release measured in other tropical river basins and across the Amazon basin[16,41].
133 They result from high dissolved concentrations of CO_2, of 22 – 86 μmol L^{-1}, average 50 ± 12
134 μmol L^{-1} (equivalent to 527 – 2600 ppm, average 1475 ± 350 ppm), combined with relatively
135 high rates of gas exchange. The average measured gas transfer velocity (Methods) k_{600} = 16
136 ± 4 m day^{-1}, towards the higher end of global river compilations[2,42] and downstream Amazon
137 River tributaries[41], but consistent with the high flow period and steeper channel slopes
138 associated with the Andes mountains and Amazon foreland floodplain[43].

The measured CO_2 release remained high from the mountains to lowland floodplain rivers, with CO_2 release increasing downstream as cumulative channel area increased (Table S1). The measured CO_2 release is large in comparison to the instantaneous DIC flux. At the largest drainage area downstream, the instantaneous upstream CO_2 release (2360 mol s^{-1}) is similar to the river DIC flux (2420 mol s^{-1}) in the wet season (Table S2) and suggests the CO_2 losses are equivalent to ~98% of the DIC export. At the Rio Manu and Rio Alto Madre de Dios the cumulative upstream CO_2 losses are also high, at 26% and 75% of the instantaneous DIC flux, respectively.

A reach-scale flux balance (Methods, Table S2) reveals a notable net loss of DIC downstream during the wet season (Fig. 1B). The fluxes of dissolved Na^+ and K^+, which are mostly derived from silicate mineral weathering[38], have negligible change downstream. Along this reach, the instantaneous sediment flux increased 10 ± 7 %. Increased sediment flux is likely to derive from Andean-fed inputs, active floodplain migration[44] and alluvial gold mining in the upstream Rio Colorado[45,46] that are eroding soil and mobilising floodplain sediment (Fig. 1A). In contrast, the combined instantaneous DIC flux of the inputs was larger than downstream DIC flux on the Rio Madre de Dios (2420 ± 120 mol s^{-1}). This loss of DIC (-620 ± 180 eq s^{-1}) is equivalent to -21 ± 6 % of the upstream DIC inputs (Fig. 1B; Table S2) and is coincident with an apparent instantaneous flux decrease of -400 ± 210 eq s^{-1} of Ca^{2+}, alongside Mg^{2+} loss. In the dry season, the reach behaves differently, with a net downstream increase in Ca^{2+}, Mg^{2+} and residual negative charge (assumed to be dominated by HCO_3^-), of about half the magnitude of the wet season losses (Table S2, Fig. 1B). The large-scale transient losses of river CO_2 and changes in DIC and cation fluxes suggest a dynamic biogeochemical system. To understand the drivers and consequences we need to first assess the source of CO_2 inputs from the landscape and during river transport.

Isotopic insight on river CO_2 and DIC inputs from organic matter respiration

Previous work on the rivers of the Amazon Basin interpreted radiocarbon measurements on DIC to suggest that CO_2 released from rivers was very young, originating from organic matter formed less than five years prior to sampling[9]. However, in that work, sites where significant carbonate weathering inputs were suspected were not included, with dissolved ion data not available to help account for the million-year old $CaCO_3$-derived DIC. These included locations in the upper Rio Maderia and the Rio Beni sampled in 1994 and 1996 (Fig. 2A & B), the neighbouring tributary to the Madre de Dios. $F^{14}C$ measurements on evaded river CO_2 from the lowland Madre de Dios Basin from 2012[47] were interpreted as reflecting carbonate weathering inputs, in addition to CO_2 sourced from organic matter formed before 1955.

Here, we find river CO_2 and DIC from the Andes to the Amazon floodplain was ^{14}C-depleted compared to the atmosphere (Fig. 2) and generally consistent with the range of values measured in the adjacent Rio Beni catchment (Fig. 2A), also fed from the erosive, sedimentary-rock bearing Andes. The CO_2 carried in the main stem of the Madre de Dios downstream had a $F^{14}C$ value of 0.809 that was very similar to the larger DIC pool (Methods, Table S3) and CO2 F14C values in the main tributaries (Manu, Alto Madre de Dios). The highest $F^{14}C$ values of CO_2 ($F^{14}C$ = 0.954) and DIC ($F^{14}C$ = 0.923) measured in the lowland Rio Los Amigos that drains only floodplain. These values suggest some input of ^{14}C-depleted DIC in all rivers, which could reflect some combination of rock-derived inputs (carbonate minerals, rock organic matter oxidation) that are known to be important weathering processes[38,40], or other aged organic matter sources in soils and sediments[18,47].

To quantify the source and age of river CO_2 inputs, we quantify chemical weathering[48] alongside the known important role of organic matter respiration in tropical river systems[2,8,16,47]. Silicate mineral weathering by carbonic acid produces dissolved cations and draws down CO_2 at the reaction site into the DIC pool, dominantly as the bicarbonate ion (HCO_3^-,). In parallel, carbonate minerals hosted in rocks can be dissolved by CO_2-rich soil porewaters or stronger acids[49–51] and deliver cations Ca^{2+} (and Mg^{2+}) alongside HCO_3^-. A portion of this DIC represents contemporary CO_2 drawdown, while the remainder is geological in age. In the case of this region of the Andes, Paleozoic sedimentary and metasedimentary rocks are widespread and carbonate mineral weathering dominates the delivery of cations and DIC to river systems[38], in analogy with many catchments around the world[3].

Alongside DIC inputs from carbonate minerals, the input of DIC supplied via respiration (and/or exchange with the atmosphere) can be assessed using isotope mass balance [48]. To do so, it is necessary to account for both the river DIC flux (Q_{DIC}, mol s^{-1}) and the flux of CO_2 emitted from the combined upstream channel area, F_{CO2} (mol s^{-1}) (Methods)[18,52], where the total DIC flux ($Q_{DIC\text{-}total}$, mol s^{-1}) at a point in a river system is described as:

$$Q_{DIC-t} = Q_{DIC} + F_{CO2} + Q_{SC} \qquad \text{(Equation 1)}$$

where Q_{SC} is a loss of DIC to secondary carbonate precipitation. The very low particulate inorganic carbon (PIC) concentration in river sediments of the downstream sites (~0.01 weight %, Table S5) suggests Q_{SC} is small and we do not account for it here. The sources of this total DIC can then be modelled as either carbonate mineral derived (i.e. millions of years old) or derived from respiration of OM (Methods). This OM can range in age dramatically, with rapidly cycling OM delivering CO_2 via autotropic and heterotrophic respiration on DOC and POC which may be a matter of years old[8], while older stores in biomass and soils can contribute decadal-aged C, and potentially centennial to millennial aged carbon[18,47,48]. Rock organic

matter weathering can also release CO_2 in the weathering zone[53] and trace element proxies suggest this is an important source of CO_2 in the Madre de Dios Basin[40].

The measured radiocarbon and stable isotope composition of river DIC and CO_2 (Table S3) requires a large and sustained CO_2 supply from OM respiration. Based on the contributions of DIC from silicate and carbonate mineral weathering, and scenarios capturing the potential fate of CO_2 and role of sulfide mineral oxidation, we calculate a range of plausible values of the radiocarbon and stable isotope composition of the non-carbonate mineral sourced DIC ($F^{14}C_{non\text{-}CaCO3}$ and $\delta^{13}C_{non\text{-}CaCO3}$, Methods). In line with previous work, carbonate mineral weathering is an important contributor, and we estimate the fraction of the total DIC pool (DIC + CO_2 lost to evasion) from $CaCO_3$ minerals ranged from ~0.10 to 0.25 (Table S4). In the main channel of the Rio Madre de Dios, the non-carbonate sourced DIC (Fig. 3A) have estimated $F^{14}C_{non\text{-}CaCO3}$ values of 1.02 – 1.12 (the interquartile range of estimates) and $\delta^{13}C_{non\text{-}CaCO3}$ of between -21.8 ‰ to -20.9 ‰ (Table S4). These $F^{14}C_{non\text{-}CaCO3}$ values are similar to estimates upstream in the Manu (1.05 – 1.17) and Alto Madre de Dios (0.99 – 1.09). In the floodplain river, Rio Los Amigos, the $F^{14}C_{non\text{-}CaCO3}$ values were higher 1.18 – 1.29 and $\delta^{13}C_{non\text{-}CaCO3}$ values ~-25 ‰ (Table S4). The stable isotope composition is consistent with an OM source of CO_2 in surface soils and relatively minor direct contributions from atmospheric CO_2 ($\delta^{13}C_{atmosphere}$ -8.2 ‰) (Fig. 2B). The calculated $F^{14}C_{non\text{-}CaCO3}$ values at these downstream and lowland sites are generally higher than the atmosphere in the year of sampling (2019, $F^{14}C_{atmosphere}$ = 1.02)[54]. This requires inputs from OM in biomass and soil that retains the elevated ^{14}C signature of the “bomb spike” (Fig. 3A). In the Andes and at the mountain front, we estimate lower potential $F^{14}C_{non\text{-}CaCO3}$ values down to ~0.90 and recognise that this itself is a mixture of potential carbon sources (Table S4).

The seminal work on river CO_2 emissions in the Amazon Basin concluded that they were fuelled by supply of CO_2 from OM that was less than 5 years old in the lowland, where the signature of $CaCO_3$-drived DIC was deemed negligible[2]. Our data show rivers in the Andean adjacent floodplains cycle carbon older than 5 years old into CO_2. The $F^{14}C_{non\text{-}CaCO3}$ values (Fig. 3A) in the lowland Rio Los Amigos are equivalent to organic matter formed from atmosphere between ~40 to ~50 years before the sampling period[54], while the main stem the values are equivalent to organic matter formed up to ~20 years prior. At the Andes mountain front, the $F^{14}C_{non\text{-}CaCO3}$ values suggest older OM may be important. The input of CO_2 from rock OM oxidation is highest within 50 km of the mountain front[40], and so could explain some ^{14}C-depletion. It could also be sourced from the degradation of OM found in the deep organic rich soils of the Kosnipata river basin and that are eroded and carried in river sediments and the POC load[55,56]. By accounting for carbonate weathering inputs and the instantaneous DIC flux

and CO_2 release (Methods) we therefore find evidence for decadal-aged, biosphere-derived OM contributing to high rates of CO_2 emission.

River DIC losses linked to water-sediment interactions

Given the backdrop of high rates of CO_2 evasion, equivalent to up to 98% of the river DIC pool, it is important to understand how this could impact the security of the river DIC pool during downstream transit. During the wet season, the reach-scale instantaneous mass balance shows -21 ± 6 % loss of DIC (Fig. 1B), while other cations (Na^+) did not decline (Table S2). In the dry season, the reach scale mass balance shows an increase in DIC downstream, albeit about half of the dry season loss (Fig. 1B, Table S2). The wet season DIC loss presents a geochemical conundrum: it is not solely a CO_2 loss, but a decrease in the anion HCO_3^- that must have other consequences. To compensate for the loss of HCO_3^- and negative charge, there are three mechanisms of note to discuss: i) secondary carbonate precipitation; ii) continued pyrite mineral weathering and sulfuric acid addition; iii) cation exchange reactions.

The reach scale mass balance shows a decline in Ca^{2+} flux downstream, of -200 ± 110 mol s^{-1} (or -13 ± 7 %) and Mg^{2+} of -25 ± 20 mol s^{-1} (or -8 ± 6 %) which is roughly half of the DIC flux decline of -620 ± 180 mol s^{-1} (Fig. 1B). This decline would be consistent with secondary carbonate precipitation, with the stoichiometry of Ca^{2+} loss to HCO_3^- (or DIC) loss of ~ 1:2. However, given the pH, temperature, DIC and alkalinity of the river water, we calculate that the calcite saturation index, $SI_{calcite}$ is -0.9 in the Manu and -1.4 in the main stem Madre de Dios (Methods, Supplementary Table S3). This is much lower than calcite saturation ($SI_{calcite}$ = 0) and much lower than river water which is inferred to be super-saturated with respect to calcite up to $SI_{calcite}$ ~ 1 [24,29]. We further examine evidence for secondary carbonates in the river sediment load using $F^{14}C$ values of particulate inorganic carbon (PIC) (Table S5). The lowland river suspended loads have an elevated $F^{14}C_{PIC}$ = 0.14 (Fig. 2B) compared to that expected for detrital carbonate ($F^{14}C_{PIC}$ ~ 0). Any secondary carbonate would have the $F^{14}C$ value of river DIC ~0.80. Considering a binary mixture of the DIC pool and detrital carbonate, the measured values suggesting this mechanism, albeit that the detrital $CaCO_3$ is still the major pool in the river sediments. There could be higher PIC contributions in riverbed materials which can have altered pore water chemistry. However, the PIC concentration is very low in exported river sediments (~0.01%), with an estimated instantaneous flux of secondary PIC of ~9 mol s^{-1} that is ~1 % of the DIC loss. Secondary carbonate formation cannot be playing a major role.

The continued oxidation of detrital pyrite across the floodplain reach could drive DIC loss via supply of H_2SO_4:

279 $$2HCO_3^- + H_2SO_4 + X^{2+} = 2CO_2 + 2H_2O + SO_4^{2-} + X^{2+}$$ (Equation 2)

280 where X^{2+} represents charge from cations in the water. An important role of continued pyrite
281 oxidation is supported by the downstream increase in instantaneous dissolved SO_4^{2-} flux of +
282 8 ± 6 % (Table S2). Paired S and O isotopes of SO_4^{2-} in these samples also support this
283 mechanism[39], indicating pyrite oxidation as the primary SO_4^{2-} source. These findings suggest
284 that sulfuric acid could titrate the DIC pool of large rivers and drive CO_2 loss that contributes
285 to contemporary river CO_2 emissions. However, the SO_4^{2-} flux increase of 14 ± 10 mol s^{-1} can
286 explain only ~5 % of the DIC losses via this mechanism, and sulfide oxidation cannot explain
287 the decrease of the instantaneous Ca^{2+} flux downstream (Fig. 1B).

288 We propose that cation exchange on charged particle surfaces could play a major role
289 in driving DIC loss during the wet season sampling, caused by rapid changes in water-solid
290 equilibrium reactions (Fig. 3B). Clay minerals, colloids and organic matter have negatively
291 charged sites on their particle surfaces which can transiently host and exchange cations and
292 protons. Cation exchange can remove Ca^{2+}, while releasing other cations such as Na^+, or H^+
293 ions [31,57,58].

294 $$Ca^{2+} + 2HCO_3^- \rightleftharpoons 2H^+ + 2HCO_3^- \rightleftharpoons 2CO_2 + 2H_2O$$ (Equation 3)

295 Exchange of protons for Ca^{2+} on colloids, mineral surfaces and DOC could thus operate to
296 drive a 1:2 ratio of Ca^{2+} loss to CO_2 degassing in analogy with process happening in soils,
297 where water-particle contact times are longer[32].

298 The cation exchange capacity in rivers is strongly correlated with suspended sediment
299 concentration (SSC) [31] and likely to be bolstered by high POC and DOC loads in Amazon
300 River tributaries [10,59–61]. For the wet season Rio Madre de Dios, a high SSC of between 1610
301 mg L^{-1} (at 2 meters water depth) and 4680 mg L^{-1} (10 meters) could result in an exchangeable
302 Ca^{2+} pool equal to ~10-30% of the dissolved Ca^{2+} pool[31]. This provides a large enough pool to
303 explain the magnitude and ratio of Ca^{2+} and DIC loss along the instantaneous reach flux
304 measurements (Table S2). An important role for cation exchange on particles is also supported
305 by the lack of measured change in dissolved ion fluxes downstream during the dry season
306 (May 2019). At this time of year, sediment concentrations and fluxes are lower as rainfall-
307 driven and riverbank erosion decrease.

308 The inorganic driver of DIC loss via cation exchange during the wet season may be
309 intimately linked to organic matter degradation and CO_2 supply, alongside CO_2 release in this
310 river, that act as a lever on water pH, and could lead to dynamic changes in particle-water
311 exchange equilibria. Experiments and semi-empirical models suggest a pH-dependence of
312 both Ca^{2+} uptake to particle surfaces and the relative competition between H+ and Ca^{2+} for
313 surface exchange sites [58,62]. At dissolved Ca^{2+} concentrations similar to measured here (~400

μmol L^{-1}), the proportion of dissolved Ca^{2+} on DOC and mineral surfaces is predicted to increase ~2-3 times between pH 6 and 8, while the H^+/Ca^{2+} ratio of ions on surfaces is predicted to decline. As such, the continued CO_2 release along this reach, and its impact in reducing H_2CO_3, could increase pH and influence the cation exchange dynamics in a way that causes a decline in pH and release of CO_2 (Equation 3). These cryptic secondary processes have not been measured directly in this, or other, river systems. Nevertheless, our findings suggest cation exchange could be a major driver of net DIC loss in this large tropical river.

DISCUSSION

Implications for the security of river DIC export

To limit the impacts of future climate change, reductions in CO_2 emission are critical but may not be possible for industries that are hard to decarbonise[63]. As such, there is a pressing need for CO_2 removal strategies that can be deployed at scale and that can achieve secure and permanent storage of CO_2. ERW holds promise and has been the subject of large-scale trials[25], while direct RAE is an emerging field of research, albeit one which companies are applying it to achieve CO_2 removal[23]. The CO_2 drawdown achieved by the carbon management technologies of ERW and RAE require the increase of stream and river cation loads and the secure export of DIC and cations to the ocean[28]. While CO_2 release from river surfaces is known to be a major carbon flux[2], if it is supplied from organic matter respiration[18] it cannot alone act to decrease the net DIC export that is set by the cation and anion load derived from chemical weathering and atmospheric inputs[24].

Model studies suggest that rivers do have the geochemical capacity to transport a sizable increase in DIC flux to the ocean[30], albeit with an upper limit where carbonate precipitation could be triggered in river waters[24]. For UK rivers, it has been estimated[29] that carbonate precipitation could lead to a 16-27% reduction in CO_2 removal potential of ERW at the application rates necessary to impact national carbon budgets. However, the potential of cation exchange processes in driving DIC loss in rivers has not been assessed. Cation exchange reactions are a well-known feature of global river systems and argued as a major sink of Ca^{2+} (and source of Na^+) in rivers around the world[31]. These processes could play an unseen role in the modern-day land to ocean riverine carbon transfer[6], while being modified by land use change and modifications to river chemistry by ERW and RAE.

Anthropogenic activities could act to increase cation exchange and drive net DIC loss from rivers. Globally, it is estimated river sediment loads have increased ~215% due to agricultural, urban and industrial land use changes[64]. For example, the Rio Colorado in our study region (Fig. 1A) has been heavily impacted by mining of alluvial floodplain deposits for

gold, involving large scale deforestation and extensive mechanical re-working of sediments proximal to river channels[46,65]. In both wet and dry seasons, the Rio Colorado has a very low Ca^{2+}/Na^{+} ratio of ~1 compared to the main stem of the Madre de Dios of 4.3[40] and we found that CO_2 release was higher downstream of its confluence (Table S1). This hints that large scale disturbance of sediment loads could result in cation exchange that impacts the river dissolved load [31] and the DIC pool in the Rio Colorado. Secondly, at the regional to global scale, anthropogenic activities may have reduced the reversibility of these reactions. In many in estuarine environments, Ca^{2+} on surfaces may be exchanged in seawater [57] and potentially drive an invasion of CO_2. However, the construction of dams and reservoirs has reduced sediment export to the ocean by 49%[64]. These observations have important implications for ERW accounting[27], which may need to either: (1) adopt a conservative assumption that any Ca^{2+} estimated to be removed by cation exchange represents a loss of CDR (e.g. analogous to current protocols in terms of soil exchangeable ions[23]), or (2) incorporate sediment transport and exchange modelling to estimate the fraction and timing of sediment delivery to oceans.

When considering the CO_2 removal achieved by ERW and RAE, our work suggests that cation exchange reactions in rivers could impact the security of DIC export over seasonal cycles lined to river sediment transport (Fig. 1A). In addition to the important role of cation exchange in soils for causing delays to CO_2 drawdown[32], we propose river sediments need to be accounted for when modelling the fate of alkalinity additions. Based on the observations made here, the best sites for ERW and RAE deployment could then also include consideration of rivers with low sediment loads, or load which has low cation exchange capacity, in addition to higher pH rivers (where exchange may have reached equilibrium). Field measurements alongside laboratory and numerical experiments are required to assess how ERW and RAE increases to cation and DIC loads could impact cation exchange in rivers and their degree of reversibility, helping to accurately account for the CO_2 drawdown that is required to reach global climate goals.

Materials and Methods

Study area

We focus on the Rio Madre de Dios which drains the Peruvian Andes to the lowland Amazon River, and is one of the major tributaries of the Rio Maderia. The basin is well characterised through a significant body of work examining hydrology [39,66,67], geomorphic processes and organic matter cycling [68,69] chemical weathering provenance and fluxes from carbonate, silicate and sulfide mineral weathering alongside rock organic matter oxidation [38,40]. The wider Amazon has also been a focus of seminal papers on river CO_2 emissions [8,9,16,41] and the use of radiocarbon to track carbon source and cycling across the basin [9,47]. Sampling focused on key locations in the river network (Fig. 1A), which include the Andean Rio Kosnipata; the Rio Alto Madre de Dios close to the mountain front; the confluence of two large Andean fed rivers, the Rio Manu and Rio Alto Madre de Dios; the Rio Los Amigos that drains only floodplain; and the downstream Madre de Dios at Dios at the Los Amigos Biological Station (formally CICRA) (Table S1 and S2).

At these key sites, and others between them, a set of holistic hydrometric and geochemical measurements were made in March 2019 during a 6-day Andes to Amazon lowland transect. The sites were re-sampled for major ions and dissolved ion fluxes during the dry season of the same year in May 2019 [39,40].

Dissolved ions, dissolved CO_2 and river CO_2 emissions

In March and May 2019, water samples were collected from the surface of main channels using a pre-rinsed bucket, and from discrete depths near the Los Amigos Biological Station on the Rio Madre de Dios using an adapted Van Dorn sampler. The sampling methods for dissolved load chemistry are described in detail previously [40]. In summary, river water was collected into sterile gas tight cider sampling bags and stored in the dark until filtration within 6 hours of collection. Waters were filtered through 0.2 µm PES filters and stored in pre-cleaned HDPE bottles (pre-acid cleaned for cations and trace elements; and deionised water cleaned for anions) in the dark, shipped to the UK and stored at 4°C until analysis. Major cations, anions and trace elements are reported in previous studies [39,40]. In summary, the major cations and anions reported here were determined by Ion Chromatography at Durham University or University of Southern California to a precision better than 3% (Table S3). In addition, pH and water temperature were measured using hand-held probes in the field and calibrated between sample locations.

During the wet season sampling in March 2019, at 12 sites across the transect, CO_2 concentrations and surface emissions were measured. Dissolved CO_2 concentrations were measured using a headspace sampling method [70]. Using two 60mL syringes, 30mL of river

water was collected and then 30mL of ambient atmosphere added (partial pressure of CO_2, pCO_2, measured with an infrared gas analyser IRGA - PP systems EGM5). The syringes were capped and shaken for 2 minutes. The headspace was injected into the IRGA and a box function recovered to determine pCO_2, (ppm) in the headspace mixture. The IRGA was re-zeroed, using a soda lime trap to create a zero CO_2 sample before each set of injections. The dissolved CO_2 concentration in the sample was then calculated using established approaches [70] as the average of the duplicate measurements, which had an average RSD of 6%.

At 12 sites river CO_2 release (also termed river CO_2 evasion, or emission) was measured using a floating chamber method [16,41]. A chamber (surface area, $A_{chamber}$ = 0.08 m^2, chamber and sampling line volume $V_{chamber}$ = 0.023 m^3) was placed on the channel surface for 3 minutes to measure change in pCO_2 over time. The chamber was then raised and flushed with atmosphere and the measurement repeated between 3 to 6 times at each site. The measured pCO_2 accumulation rate ($\Delta pCO_2/\Delta t$, µatm s^{-1}) was calculated using a linear fit with associated uncertainty and converted to a flux of CO_2 release (F_{CO2}, mol m^{-2} s^{-1}):

$$F_{CO2} = \frac{\Delta pCO_2}{\Delta t} \cdot \frac{V_{chambe}}{(R \cdot T \cdot A_{chambe})} \quad \text{(Equation 4)}$$

where T is the temperature (ºK) and R the universal gas constant (82.057 m^3 µatm K^{-1} mol^{-1}). At the 10 sites with paired measurements of F_{CO2} and dissolved CO_2 concentration, the gas transfer velocity, *k* (m day^{-1}), was quantified using:

$$F_{CO2} = k \cdot (C_w - C_{atm}) \cdot \beta \quad \text{(Equation 5)}$$

where C_w is the dissolved CO_2 concentration in the water (µmol L^{-1}) and C_{atm} is the concentration of CO_2 (µmol L^{-1}) in a water parcel at equilibrium with CO_2 in the atmosphere at that site (Table S1) and β is a conversion factor between s and days [41].

Radiocarbon and stable isotopes of CO_2 and DIC

To constrain the isotopic composition of dissolved CO_2 and the wider river DIC pool, we focused on a method which eliminates the need for frozen water storage or use of poison in the field. The super-headspace method was used to sample the river CO_2 [71] with some modifications to aid with sample collection. During the wet season sampling campaign (March 2019), 12L of river water was collected in a gas tight cider bag and sealed with a bung. A CO_2-free headspace was added to the sample using a soda-lime cartridge and the IRGA pump. 2-3 L of headspace was added prior to rigorous shaking for 3 minutes to transfer dissolved CO_2 into the headspace [71]. The headspace was then extracted and collected onto a zeolite trap, with between 1.1 and 5.32 ml of CO_2 collected onto each sieve.

In addition to river CO_2, we also collected DIC for isotopic analysis. Here, river water collected with a syringe was filtered through a 0.2 µm PES filter into a foil bag [72]. Between

200-500 mL of sample was collected. Bags could not be refrigerated or frozen while in the field but were frozen on return to the laboratory between 3 and 9 days following collection.

The samples of CO_2 on zeolite sieves were recovered in the laboratory at the NEIF Radiocarbon Laboratory, East Kibride UK, using methods previously described [71]. For the DIC bags, pure sample CO_2 was cryogenically recovered following acid hydrolysis [72] and the DIC concentration calculated (mol L^{-1}). An aliquot of the recovered CO_2 from each sample was used for stable C isotope measurement using isotope ratio mass spectrometry (IRMS) and reported as $\delta^{13}C$ relative to VPDB. Radiocarbon was measured by accelerator mass spectrometry (AMS) following graphitisation [73] with results normalised to $\delta^{13}C$ = -25 ‰ to account for isotopic fractionation and reported as the Fraction Modem ($F^{14}C$) [74], where ^{14}C age = -8033 * Ln ($F^{14}C$).

It is uncommon to have paired measurements of $F^{14}C$-DIC and $F^{14}C$-CO_2 from river systems. The equilibration of CO_2 and HCO_3^- in aqueous solutions is typically between 20-200 s [75] which can be viewed as quick in the reference frame water residence times in catchments, which are of the order of days or longer [76]. However, in laboratory experiments, isotopic equilibrium between CO_2 and HCO_3^- is longer, at ~1-2 hours [77]. While still fast compared to mixing of waters in rivers, it is not instantaneous, and there could be river settings where CO_2 supply from respiration of tributaries does not mix as quickly with the DIC pool.

A published assessment of available data showed that the $F^{14}C$-CO_2 and $F^{14}C$-DIC values of streams, rivers and lakes were generally in close agreement for a range of pH values from 6 to 9, with a mean difference of 0.02 [18]. At pH ~6-7, $F^{14}C$-CO_2 was generally slightly higher than DIC, by ~0.01-0.04. Four of the five paired CO_2 and DIC samples taken here showed a similar pattern, with $F^{14}C$-CO_2 higher by 0.0298, which is higher than analytical uncertainty (Table S3). This is interesting and suggests the potential for some systematic offset between CO2 and DIC, albeit small, in these tropical rivers. At one of our sites (Rio Alto Madre de Dios at the mountain front) the difference was larger, with $F^{14}C$-CO_2 0.0923 higher than the corresponding $F^{14}C$-DIC measurement (Table S3). This site is found where several tributaries meet and mix in a reach where steeper, gravel bed river sections of the river system are still present close to the Andes front that cause a large degree of internal and surface water turbulence at high flow. We speculate that these geomorphic features could lead to greater disequilibrium between the dissolved carbon species in the river, and manifest as a higher (more modern) $F^{14}C$-CO_2 value than the bulk DIC. Further work should explore these interesting observations in a larger number of river basins. Given the good agreement between CO_2 and DIC for the other sites, we focus our analysis on the CO_2 measurements for all sites.

Radiocarbon and stable isotope analysis of river POC and PIC

Measured quantities of river particulate organic carbon (POC) were decarbonated using a 'no leach' acid treatment that retained mobile organic carbon[78] and subsequently combusted to CO_2 using the sealed quartz tube method[79]. Particulate inorganic carbon (PIC) was converted to CO_2 from measured amounts of sediment using acid hydrolysis [73]. The cryogenically purified CO_2 was recovered from both sets of samples and quantified using a calibrated volume. All samples were converted to graphite using Fe-Zn reduction and measured by AMS [73], with results expressed as $F^{14}C$ as described above.

River chemistry equilibrium modelling

Calcite saturation indices were calculated using PHREEQC (Version 3)[80], with the phreeqc.dat thermodynamic database. Input chemistry included major cation concentrations (Ca^{2+}, Mg^{2+}, Na^{+}, K^{+} and Sr^{2+}), major anions (F^{-}, Cl^{-}, NO_3^{-} and SO_4^{2-}), temperature, DIC and pCO_2. Measured DIC and pCO_2 (Supplementary Table S1 & S3) were used to constrain carbonate speciation and calculate the calcite saturation index ($SI_{measured}$). Predicted pH values were on average within 0.27 pH units to measurements, and had no systematic bias to higher or lower pH. The assessment requires some negative charge deficit, which is consistent with the interpretations that DOM, colloids and mineral surfaces are playing an important role in the charge balance and equilibrium exchange chemistry of these river waters.

River channel surface area

We used the newly developed Global River Topology (GRIT)[81] as the underlying river network. GRIT contains multiple river-reach attributes, including upstream drainage area, river width and river length. River width was derived as the median value from the Global River Widths from Landsat (GRWL)[82] database for each river reach, with an approximate reach length of 1 km. Sampling sites were matched to the river network at the reach scale using a nearest-distance method. After each sampling site was linked to its corresponding river reach, the upstream river-channel surface area was calculated by summing the product of river width and reach length across all upstream river reaches.

Instantaneous water and solute fluxes

During both wet and dry season trips, instantaneous water discharge (Q_w, m^3/s) was measured using a boat mounted Acoustic Doppler Current Profiler (ADCP). Measurements were made in both trips on the Alto Madre de Dios, Chilibe, Colorado, and the downstream Madre de Dios. Unfortunately, at the Rio Manu, an instrument failure in March 2019 means that we do not have a measurement from this site, but this site was measured in May 2019. In March 2019, the Rio Manu Q_w was calculated assuming a closed Q_w balance (i.e. Manu = Madre de Dios -

Alto Madre de Dios - Chilibe – Colorado). At least two repeated channel transects were made to measure Q_w, and these had an average relative standard deviation of 3.6% and so we assume Q_w has a precision of better than ± 5%.

Instantaneous fluxes of suspended sediment and dissolved constituents (mol s^{-1}) were determined by multiplying concentrations (mg m^{-3} or mol m^{-3}) by water discharge (Table S2). A reach scale mass balance of water and dissolved constituents downstream for both seasonal sampling campaigns was represented as the percentage difference between the sum of upstream fluxes from the Rio Manu, Rio Alto Madre Dios, Rio Chilibe and Rio Colorado to the Rio Madre de Dios downstream (Table S2)

The isotopic composition of CO_2 addition via weathering partitioning

To use radiocarbon and stable carbon isotopes to better constrain the source of CO_2 input into the DIC load of these Andean to Amazon floodplain rivers, we aim to un-mix the contribution of DIC directly from the $CaCO_3$ minerals liberated during carbonate weathering for the wet season samples where all data is available. First, we model the total DIC pool (DIC_{total}, µmol L^{-1}) as the combination of the within river DIC measured at a site (DIC_{river}) plus the DIC lost as CO_2 was emitted during transport to the site ($DIC_{CO2\text{-}loss}$), alongside secondary carbonate precipitation (DIC_{SC}):

$$DIC_{total} = DIC_{river} + DIC_{CO2-loss} + DIC_{SC} \quad \text{(Equation 6)}$$

Here DIC_{SC} ~ 0 due to the very low particulate inorganic carbon concentrations (Table S5) and thus:

$$DIC_{total} = DIC_{river} + f_{CO2-los} \cdot DIC_{river} \quad \text{(Equation 7)}$$

where $f_{CO2\text{-}loss}$ is the river CO_2 loss upstream of a sampling point expressed as a fraction of the measured river DIC pool at the sampling location.

The total DIC pool can be modelled as the mixture of carbonate mineral DIC (DIC_{CaCO3}) and DIC from other carbon inputs:

$$DIC_{total} = DIC_{CaCO3} + DIC_{non-CaCO3} \quad \text{(Equation 8)}$$

$$f_{CaCO3} = \frac{DIC_{CaCO}}{DIC_{total}} \quad \text{(Equation 9)}$$

where f_{CaCO3} is the fraction of carbonate mineral derived DIC in the total DIC pool. The $DIC_{non\text{-}CaCO3}$ comprises of some combination of: i) DIC sourced from atmospheric or CO_2 during carbonate mineral weathering; ii) DIC sourced from atmospheric or CO_2 during silicate mineral weathering; iii) CO_2 inputs associated with autotropic respiration of plants and heterotrophic respiration of organic matter in soils, sediments or river waters (DOC and POC re-

mineralisation); iv) oxidation of rock organic matter; and v) invaded or exchanged CO_2 from the atmosphere.

The isotopic composition of the "non-$CaCO_3$" derived DIC can then be calculated to assess its source. We assume that the CO_2 inputs mix quickly with the existing DIC pool on the days long transport of the river water, and that the CO_2 lost has the same $F^{14}C$ value as the DIC pool [18], while remembering the $F^{14}C$ notation corrects for any stable isotope fractionation [74], then the $F^{14}C$ value of DIC pool in the river ($F^{14}C_{river}$ = $F^{14}C_{total}$) can then described as:

$$F^{14}C_{river} = f_{CaCO3} \cdot F^{14}C_{CaCO} + (1 - f_{CaCO3}) \cdot F^{14}C_{non-CaCO} \quad \text{(Equation 10)}$$

Where the million-year-old $CaCO_3$ has a $F^{14}C_{CaCO3} \sim 0$ (i.e. indistinguishable from analytical backgrounds). In contrast the stable isotope composition is complicated by isotope fractionation. The portion of DIC present as CO_2 has a lower $\delta^{13}C$ value than HCO_3^- in equilibrium (Zhang et al., 1994), meaning that CO_2 emissions can cause the DIC pool to evolve to higher $\delta^{13}C$ values. As such:

$$\delta^{13}C_{river} = (1 + f_{CO2-lo}) \cdot (f_{Ca} \cdot \delta^{13}C_{CaCO3} + (1 - f_{CaCO3}) \cdot \delta^{13}C_{non-CaCO3}) - f_{CO2-loss} \cdot \delta^{13}C_{CO} \quad \text{(Equation 11)}$$

and the isotopic composition of the non-carbonate mineral DIC can then be estimated from:

$$F^{14}C_{non-CaCO3} = \frac{F^{14}C_{river}}{(1 - f_{CaCO3})} \quad \text{(Equation 12)}$$

$$\delta^{13}C_{non-CaCO} = \left(\frac{\delta^{13}C_{river} + f_{CO2-loss} \cdot \delta^{13}C_{CO2}}{1 + f_{CO2-loss}} - f_{CaCO} \cdot \delta^{13}C_{Ca}\right) \cdot \frac{1}{(1 - f_{CaCO})} \quad \text{(Equation 13)}$$

Our measurements have constrained plausible values and ranges for $\delta^{13}C_{river}$, $F^{14}C_{river}$, $f_{CO2-loss}$, $\delta^{13}C_{CO3}$, and $\delta^{13}C_{CaCO3}$ (Table S6). The key remaining variable is thus f_{CaCO3}, the fraction of carbonate mineral-derived DIC.

To assess f_{CaCO3}, we use the dissolved ion load to assess silicate mineral and carbonate mineral weathering sources. Established forward model methods were preferred [1,40] over inversion of all dissolved ions [38] due to the primary focus here being on the potential carbonate mineral-derived DIC inputs. First, rain inputs of a dissolved ions ($[X]_{rain}$, μmol L^{-1}) to the river load were corrected using the measured composition of precipitation sampled during the study, with ratios normalised to Cl^- and the Cl^- input assumed to be dominated by precipitation inputs [40], with minimal evaporate inputs in the study area[39] where:

$$[X]^* = [X]_{river} - \left(\frac{[X]}{Cl^-}\right)_{rain} \cdot Cl^-_{river} \quad \text{(Equation 14)}$$

The precipitation contribution to the major weathering-derived ions Na^+ and Ca^{2+} concentrations was 5% and 7% on average, respectively. The precipitation contribution to SO_4^{2-} was 13% on average in the main Andean-fed sites, but was much larger in the Rio Los Amigos (92%) where the concentrations of SO_4^{2-} were very low (<1 μmol L^{-1}). It was assumed that anthropogenic inputs to major cation loads was minimal based on previous work[39,66,83] that Na* and K* were derived from silicate mineral weathering, while the contribution of Ca* and Mg* from silicate minerals, Ca_{sil} and Mg_{sil} was then estimated using:

$$Ca_{sil} = Na^* \cdot \left(\frac{Ca}{Na}\right)_{sil} \quad \text{(Equation 15)}$$

$$Mg_{sil} = Ca_{sil} \cdot \left(\frac{Mg}{Ca}\right)_{sil} \quad \text{(Equation 16)}$$

where the ratios characterise the composition of silicate minerals undergoing dissolution in the catchments[38]. The carbonate mineral contributions of Ca and Mg, were then:

$$Ca_{carb} = Ca^* - Ca_{sil} \quad \text{(Equation 17)}$$

$$Mg_{carb} = Mg^* - Mg_{sil} \quad \text{(Equation 18)}$$

The DIC contributions from silicate weathering, carbonate weathering and the $CaCO_3$ mineral specifically were then determined as:

$$DIC_{sil} = 2 \cdot Ca_{sil} + 2 \cdot Mg_{sil} + Na^* + K^* \quad \text{(Equation 19)}$$

$$DIC_{carb} = 2 \cdot Ca_{carb} + 2 \cdot Mg_{carb} - SO_{4-pyrite} \quad \text{(Equation 20)}$$

$$DIC_{CaCO3} = 0.5 \cdot DIC_{carb} \quad \text{(Equation 21)}$$

Where $SO_{4\text{-pyrite}}$ is a term which corrects for potential DIC loss associated with sulfide mineral oxidation and degassing to CO_2 and release at the reaction site [84]. As such:

$$f_{CaCO3} = \frac{DIC_{CaCO3}}{(DIC_{sil}+DIC_{carb})\cdot(1+f_{CO2-loss})} \quad \text{(Equation 22)}$$

The Equations 12 and 13 were then used to estimate $F^{14}C_{non\text{-}CaCO3}$ and $\delta^{13}C_{non\text{-}CaCO3}$ from measured constraints on the variables (Table S6). A range of values were used for each term, and a Monte Carlo approach used to return the 50th percentile and 5% to 95% percentile range of 100,000 simulated values (Table S4). In all catchments except for the Kosnipata River, the model outcomes predicted positive $fCaCO_3$ values, showing the measured and estimated values chosen for variables (Table S6) can describe the data well. In the Kosnipata, 18% of the outputs were negative values and not considered further in the analysis.

Conflict of interests: The authors declare no conflict of interests

Data availability: All data from this study is provided in the Supplementary Tables

Author contributions: RGH designed the research with AJW. RGH led the greenhouse gas measurements and sampling, RGH, AJW, EB, MD and AJCQ led fieldwork. RGH, MHG, KH, VA, MD, EB, PA, YL performed analyses and analysed data. RGH wrote the paper with inputs from all authors.

Acknowledgements: This research was funded by the European Research Council Consolidator Grant (RIV-ESCAPE, 101002563) to RGH, with additional from European Research Council (ERC) Starting Grant – ROC-CO2 (678779) to RGH and by NSF Earth Sciences award (EAR-1455352) to AJW. We thank Amazon Journeys Nature Lodges, the Amazon Conservation Association (Peru), and the Andes Biodiversity and Ecosystems Research Group (ABERG) for field support.

References

1. Galy, A. & France-Lanord, C. Weathering processes in the Ganges-Brahmaputra basin and the riverine alkalinity budget. *Chem. Geol.* https://doi.org/10.1016/S0009-2541(99)00033-9 (1999) doi:10.1016/S0009-2541(99)00033-9.

2. Raymond, P. A. *et al.* Global carbon dioxide emissions from inland waters. *Nature 2013 503:7476* **503**, 355–359 (2013).

3. Gaillardet, J., Dupré, B., Louvat, P. & Allègre, C. J. Global silicate weathering and CO2 consumption rates deduced from the chemistry of large rivers. *Chem. Geol.* https://doi.org/10.1016/S0009-2541(99)00031-5 (1999) doi:10.1016/S0009-2541(99)00031-5.

4. Hilton, R. G. & West, A. J. Mountains, erosion and the carbon cycle. *Nat. Rev. Earth Environ.* **1**, 284–299 (2020).

5. Zheng, H. *et al.* The Impacts of Erosion on the Carbon Cycle. *Reviews of Geophysics* **63**, e2023RG000829 (2025).

6. Lauerwald, R. *et al.* Inland Water Greenhouse Gas Budgets for RECCAP2: 1. State-Of-The-Art of Global Scale Assessments. *Global Biogeochem. Cycles* **37**, e2022GB007657 (2023).

7. Rocher-Ros, G. *et al.* Global methane emissions from rivers and streams. *Nature 2023 621:7979* **621**, 530–535 (2023).

8. Ward, N. D. *et al.* Degradation of terrestrially derived macromolecules in the Amazon River. *Nature Geoscience 2013 6:7* **6**, 530–533 (2013).

9. Mayorga, E. *et al.* Young organic matter as a source of carbon dioxide outgassing from Amazonian rivers. *Nature* **436**, 538–541 (2005).

10. Hedges, J. I. *et al.* Organic matter in Bolivian tributaries of the Amazon River: A comparison to the lower mainstream. *Limnol. Oceanogr.* **45**, 1449–1466 (2000).

11. Berhe, A. A., Harte, J., Harden, J. W. & Torn, M. S. The Significance of the Erosion-induced Terrestrial Carbon Sink. *Bioscience* https://doi.org/10.1641/b570408 (2007) doi:10.1641/b570408.

12. Hilton, R. G., Schwab, M. & Galy, V. Dynamics of particulate organic carbon mobilization, storage, and export across river sedimentary systems. *Treatise on Geochemistry, Third Edition, 8 Volume Set* **3**, 215–250 (2025).

13. Galy, V., Peucker-Ehrenbrink, B. & Eglinton, T. Global carbon export from the terrestrial biosphere controlled by erosion. *Nature* **521**, 204–207 (2015).

14. Cole, J. J. *et al.* Plumbing the global carbon cycle: integrating inland waters into the terrestrial carbon budget. *Ecosystems* **10**, 171–185 (2007).

15. Battin, T. J. *et al.* River ecosystem metabolism and carbon biogeochemistry in a changing world. *Nature* **613**, 449–459 (2023).

16. Richey, J. E., Melack, J. M., Aufdenkampe, A. K., Ballester, V. M. & Hess, L. L. Carbon dioxide evasion from central Amazonian wetlands as a significant source of atmospheric CO2 in the tropics. *Nature* **416**, 617–620 (2002).

17. Regnier, P., Resplandy, L., Najjar, R. G. & Ciais, P. The land-to-ocean loops of the global carbon cycle. *Nature* **603**, 401–410 (2022).

18. Dean, J. F. *et al.* Old carbon routed from land to the atmosphere by global river systems. *Nature 2025 642:8066* **642**, 105–111 (2025).

19. Broecker, W. S. Glacial to interglacial changes in ocean chemistry. *Prog. Oceanogr.* **11**, 151–197 (1982).

20. Seifritz, W. CO2 disposal by means of silicates. *Nature* **345**, 486 (1990).

21. Hartmann, J. *et al.* Enhanced chemical weathering as a geoengineering strategy to reduce atmospheric carbon dioxide, supply nutrients, and mitigate ocean acidification. *Reviews of Geophysics* **51**, 113–149 (2013).

22. Beerling, D. J. *et al.* Potential for large-scale CO2 removal via enhanced rock weathering with croplands. *Nature 2020 583:7815* **583**, 242–248 (2020).

23. River Alkalinity Enhancement v1.0 — Isometric. https://registry.isometric.com/protocol/river-alkalinity-enhancement/1.0/ctn_1JQ8ZCFJY1S0ZWXH.

24. Knapp, W. J. & Tipper, E. T. The efficacy of enhancing carbonate weathering for carbon dioxide sequestration. *Frontiers in Climate* **4**, 928215 (2022).

25. Beerling, D. J. *et al.* Enhanced weathering in the US Corn Belt delivers carbon removal with agronomic benefits. *Proceedings of the National Academy of Sciences* **121**, e2319436121 (2024).

26. Renforth, P. & Henderson, G. Assessing ocean alkalinity for carbon sequestration. *Reviews of Geophysics* **55**, 636–674 (2017).

27. Schiedung, M. *et al.* Uncertainties of enhanced rock weathering for climate-change mitigation. *Nature Reviews Earth & Environment 2026 7:4* **7**, 253–266 (2026).

28. Isson, T. & West, A. J. Can enhanced alkalinity store carbon durably? *Science (1979).* **392**, 808–810 (2026).

29. Harrington, K. J., Hilton, R. G. & Henderson, G. M. Implications of the riverine response to enhanced weathering for CO2 removal in the UK. *Appl. Geochem.* **152**, 105643 (2023).

30. Zhang, S. *et al.* River chemistry constraints on the carbon capture potential of surficial enhanced rock weathering. *Limnol. Oceanogr.* **67**, S148-57 (2022).

31. Tipper, E. T. *et al.* Global silicate weathering flux overestimated because of sediment-water cation exchange. *Proc. Natl. Acad. Sci. U. S. A.* **118**, (2020).

32. Kanzaki, Y. *et al.* Soil cation storage is a key control on the carbon removal dynamics of enhanced weathering. *Environmental Research Letters* **20**, 074055 (2025).

33. Kemeny, P. C. *et al.* Arctic Permafrost Thawing Enhances Sulfide Oxidation. *Global Biogeochem. Cycles* **37**, e2022GB007644 (2023).

34. Walsh, E. V., Hilton, R. G., Tank, S. E. & Amos, E. Temperature sensitivity of the mineral permafrost feedback at the continental scale. *Science Advances* **10**, 4893 (2024).

35. Raymond, P. A. & Oh, N. H. Long term changes of chemical weathering products in rivers heavily impacted from acid mine drainage: Insights on the impact of coal mining on regional and global carbon and sulfur budgets. *Earth Planet. Sci. Lett.* **284**, 50–56 (2009).

36. Harrington, K. J., Henderson, G. M. & Hilton, R. G. Current rates of CO2 removal due to rock weathering in the UK. *Science of The Total Environment* **957**, 177458 (2024).

37. Hotchkiss, E. R. *et al.* Sources of and processes controlling CO2 emissions change with the size of streams and rivers. *Nat. Geosci.* **8**, 696–699 (2015).

38. Torres, M. A. *et al.* The acid and alkalinity budgets of weathering in the Andes–Amazon system: Insights into the erosional control of global biogeochemical cycles. *Earth Planet. Sci. Lett.* https://doi.org/10.1016/j.epsl.2016.06.012 (2016) doi:10.1016/j.epsl.2016.06.012.

39. Burt, E. I. *et al.* Conservative transport of dissolved sulfate across the Rio Madre de Dios floodplain in Peru. *Geology* **49**, (2021).

40. Dellinger, M. *et al.* High rates of rock organic carbon oxidation sustained as Andean sediment transits the Amazon foreland-floodplain. *Proc. Natl. Acad. Sci. U. S. A.* **120**, e2306343120 (2023).

41. Sawakuchi, H. O. *et al.* Carbon dioxide emissions along the lower Amazon River. *Front. Mar. Sci.* **4**, 234365 (2017).

42. Raymond, P. A. *et al.* Scaling the gas transfer velocity and hydraulic geometry in streams and small rivers. *Limnol. Oceanogr. Fluids Environ.* **2**, 41–53 (2012).

43. Rexroade, A. T., Wallin, M. B. & Duvert, C. Measuring Gas Transfer Velocity in a Steep Tropical Stream: Method Evaluation and Implications for Upscaling. *J. Geophys. Res. Biogeosci.* **130**, e2024JG008420 (2025).

44. Constantine, J. A., Dunne, T., Ahmed, J., Legleiter, C. & Lazarus, E. D. Sediment supply as a driver of river meandering and floodplain evolution in the Amazon Basin. *Nature Geoscience 2014 7:12* **7**, 899–903 (2014).

45. Dethier, E. N. *et al.* A global rise in alluvial mining increases sediment load in tropical rivers. *Nature 2023 620:7975* **620**, 787–793 (2023).

46. Dethier, E. N., Sartain, S. L. & Lutz, D. A. Heightened levels and seasonal inversion of riverine suspended sediment in a tropical biodiversity hot spot due to artisanal gold mining. *Proceedings of the National Academy of Sciences* **116**, 23936–23941 (2019).

47. Vihermaa, L. E., Waldron, S., Garnett, M. H. & Newton, J. Old carbon contributes to aquatic emissions of carbon dioxide in the Amazon. *Biogeosciences* **11**, 3635–3645 (2014).

48. Dasari, S., Garnett, M. H. & Hilton, R. G. Leakage of old carbon dioxide from a major river system in the Canadian Arctic. *PNAS Nexus* **3**, (2024).

49. Calmels, D., Gaillardet, J. & François, L. Sensitivity of carbonate weathering to soil CO2 production by biological activity along a temperate climate transect. *Chem. Geol.* **390**, 74–86 (2014).

50. Calmels, D., Gaillardet, J., Brenot, A. & France-Lanord, C. Sustained sulfide oxidation by physical erosion processes in the Mackenzie River basin: Climatic perspectives. *Geology* https://doi.org/10.1130/G24132A.1 (2007) doi:10.1130/G24132A.1.

51. Gaillardet, J., Calmels, D., Romero-Mujalli, G., Zakharova, E. & Hartmann, J. Global climate control on carbonate weathering intensity. *Chem. Geol.* **527**, 118762 (2019).

52. Larsen, W. J. *et al.* Limited Headwater CO2 Emissions Relative to Downstream C Fluxes: Insights From a Tracer-Enabled Reactive Transport Model. *J. Geophys. Res. Biogeosci.* **130**, e2024JG008592 (2025).

53. Zondervan, J. R. *et al.* Rock organic carbon oxidation CO2 release offsets silicate weathering sink. *Nature* **623**, 329–333 (2023).

54. Hua, Q. *et al.* ATMOSPHERIC RADIOCARBON FOR THE PERIOD 1950–2019. *Radiocarbon* **64**, 723–745 (2022).

55. Clark, K. E. *et al.* New views on 'old' carbon in the Amazon River: Insight from the source of organic carbon eroded from the Peruvian Andes. *Geochemistry, Geophysics, Geosystems* **14**, (2013).

56. Clark, K. E. *et al.* Erosion of organic carbon from the Andes and its effects on ecosystem carbon dioxide balance. *J. Geophys. Res. Biogeosci.* **122**, (2017).

57. Sayles, F. L. & Mangelsdorf, P. C. The equilibration of clay minerals with sea water: exchange reactions. *Geochim. Cosmochim. Acta* **41**, 951–960 (1977).

58. Kinniburgh, D. G. *et al.* Ion binding to natural organic matter: competition, heterogeneity, stoichiometry and thermodynamic consistency. *Colloids Surf. A Physicochem. Eng. Asp.* **151**, 147–166 (1999).

59. Pérez, M. A. P., Moreira-Turcq, P., Gallard, H., Allard, T. & Benedetti, M. F. Dissolved organic matter dynamic in the Amazon basin: Sorption by mineral surfaces. *Chem. Geol.* **286**, 158–168 (2011).

60. Bouchez, J. *et al.* Source, transport and fluxes of Amazon River particulate organic carbon: Insights from river sediment depth-profiles. *Geochim. Cosmochim. Acta* **133**, (2014).

61. Rosengard, S. Z. *et al.* The Thermal Reactivity and Molecular Diversity of Particulate Organic Carbon in the Amazon River Mainstem. *J. Geophys. Res. Biogeosci.* **130**, e2024JG008660 (2025).

62. Benedetti, M. F., Milne, C. J., Kinniburgh, D. G., Van Riemsdijk, W. H. & Koopal, L. K. Metal Ion Binding to Hemic Substances: Application of the Non-Ideal Competitive Adsorption Model. *Environ. Sci. Technol.* **29**, 446–457 (1995).

63. Intergovernmental Panel on Climate Change (IPCC). Technical Summary. *Climate Change 2021 – The Physical Science Basis* 35–144 (2023) doi:10.1017/9781009157896.002.

64. Syvitski, J. *et al.* Earth's sediment cycle during the Anthropocene. *Nat. Rev. Earth Environ.* **3**, 179–196 (2022).

65. Dethier, E. N. *et al.* A global rise in alluvial mining increases sediment load in tropical rivers. *Nature 2023 620:7975* **620**, 787–793 (2023).

66. Burt, E. I., Coayla Rimachi, D. H., Ccahuana Quispe, A. J., Atwood, A. & West, A. J. Isotope-derived young water fractions in streamflow across the tropical Andes mountains and Amazon floodplain. *Hydrol. Earth Syst. Sci.* **27**, 2883–2898 (2023).

67. Clark, K. E. *et al.* The hydrological regime of a forested tropical Andean catchment. *Hydrol. Earth Syst. Sci.* **18**, (2014).

68. Clark, K. E. *et al.* Storm-triggered landslides in the Peruvian Andes and implications for topography, carbon cycles, and biodiversity. *Earth Surface Dynamics* **4**, 47–70 (2016).

69. Clark, K. E. *et al.* Erosion of organic carbon from the Andes and its effects on ecosystem carbon dioxide balance. *J. Geophys. Res. Biogeosci.* https://doi.org/10.1002/2016JG003615 (2017) doi:10.1002/2016JG003615.

70. Åberg, J. & Wallin, M. B. Evaluating a fast headspace method for measuring DIC and subsequent calculation of pCO2 in freshwater systems. *Inland Waters* **4**, 157–166 (2014).

71. Garnett, M. H., Billett, M. F., Gulliver, P. & Dean, J. F. A new field approach for the collection of samples for aquatic 14CO2 analysis using headspace equilibration and molecular sieve traps: the super headspace method. *Ecohydrology* **9**, 1630–1638 (2016).

72. Bryant, C. L. *et al.* Storage and Hydrolysis of Seawater Samples for Inorganic Carbon Isotope Analysis. *Radiocarbon* **55**, 401–409 (2013).

73. Ascough, P. *et al.* 14C MEASUREMENT OF SAMPLES FOR ENVIRONMENTAL SCIENCE APPLICATIONS AT THE NATIONAL ENVIRONMENTAL ISOTOPE FACILITY (NEIF) RADIOCARBON LABORATORY, SUERC, UK. *Radiocarbon* **66**, 1020–1031 (2024).

74. Reimer, P. J., Brown, T. A. & Reimer, R. W. Discussion: Reporting and Calibration of Post-Bomb 14C Data. *Radiocarbon* **46**, 1299–1304 (2004).

75. Zhang, J., Quay, P. D. & Wilbur, D. O. Carbon isotope fractionation during gas-water exchange and dissolution of CO2. *Geochim. Cosmochim. Acta* **59**, 107–114 (1995).

76. Collins, E. L. *et al.* Global patterns in river water storage dependent on residence time. *Nature Geoscience 2024 17:5* **17**, 433–439 (2024).

77. Szaran, J. Achievement of carbon isotope equilibrium in the system HCO_3^- (solution)-CO_2(gas). *Chem. Geol.* **142**, 79–86 (1997).

78. Garnett, M. H. *et al.* Carbonate removal from radiocarbon samples using a 'no leach' acid pretreatment to retain mobile organic carbon. *Radiocarbon*, in press (2026).

79. Boutton, T. W. *et al.* Comparison of quartz and Pyrex tubes for combustion of organic samples for stable carbon isotope analysis. *Anal. Chem.* **55**, 1832–1833 (2002).

80. Parkhurst, D. L. & Appelo, C. A. J. Description of input and examples for PHREEQC version 3: A computer program for speciation, batch-reaction, one-dimensional transport, and inverse geochemical calculations. *Techniques and Methods* https://doi.org/10.3133/TM6A43 (2013) doi:10.3133/TM6A43.

81. Wortmann, M. *et al.* Global River Topology (GRIT): A Bifurcating River Hydrography. *Water Resour. Res.* **61**, e2024WR038308 (2025).

82. Allen, G. H. & Pavelsky, T. M. Global extent of rivers and streams. *Science (1979).* **361**, 585–588 (2018).

83. Dellinger, M. *et al.* High rates of rock organic carbon oxidation sustained as Andean sediment transits the Amazon foreland-floodplain. *Proc. Natl. Acad. Sci. U. S. A.* **120**, (2023).

84. Soulet, G. *et al.* Temperature control on CO_2 emissions from the weathering of sedimentary rocks. *Nat. Geosci.* **14**, 665–671 (2021).

Figures

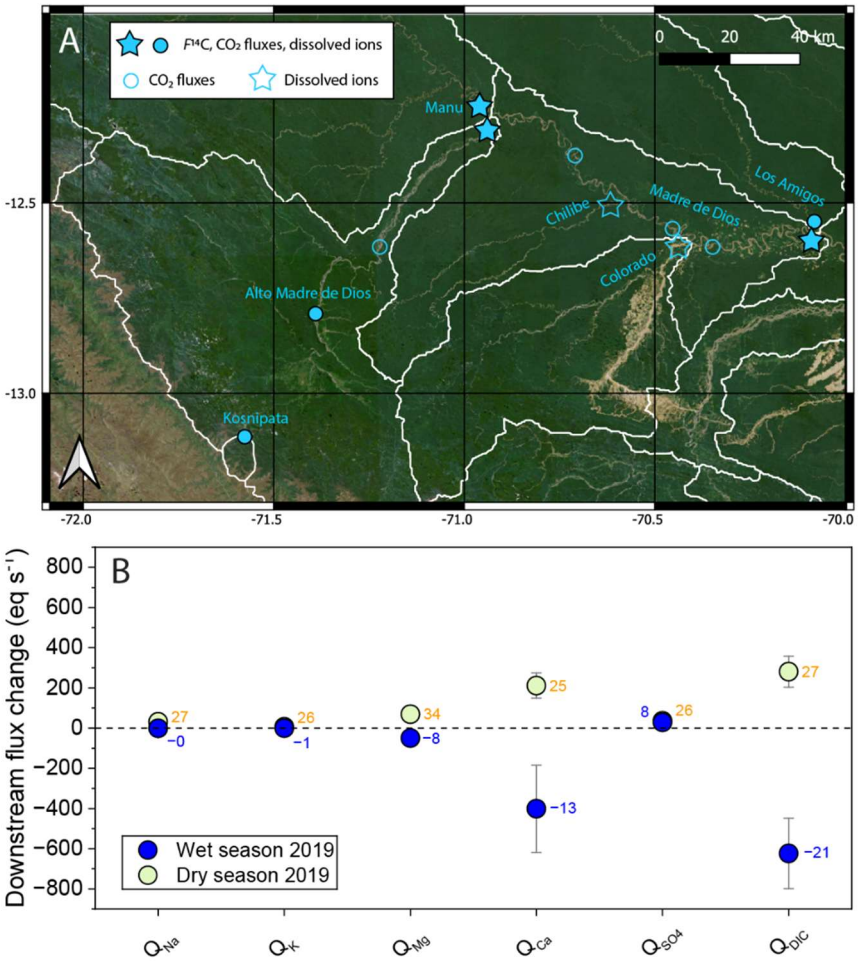

Figure 1: River DIC and CO_2 release from the Andes to Amazon floodplain in the Madre de Dios Basin. A) Satellite image of the study area (Sentinel-2 2019/04/01 mosaic) and major subbasins (white outline). Main sampling locations are shown as filled symbols, where stars indicate all measurements were made (dissolved ions, water discharge, dissolved fluxes, CO_2 release, dissolved CO_2 concentrations, CO_2 and DIC radiocarbon and stable isotopes) and circles are locations where water discharge measurements were not made. Open circles are sites where CO_2 release and concentration were determined and open stars where water discharge and dissolved ions were measured. **B)** Downstream instantaneous flux change measured in the wet (blue) and dry (yellow) seasons considering the difference between the lowland Madre de Dios site, and the sum of the upstream sites (Alto Madre de Dios, Manu, Chilibe and Colorado). Positive indicates an increase, and negative is a decrease in flux. Numbers provide the percentage loss or gain compared to the input fluxes.

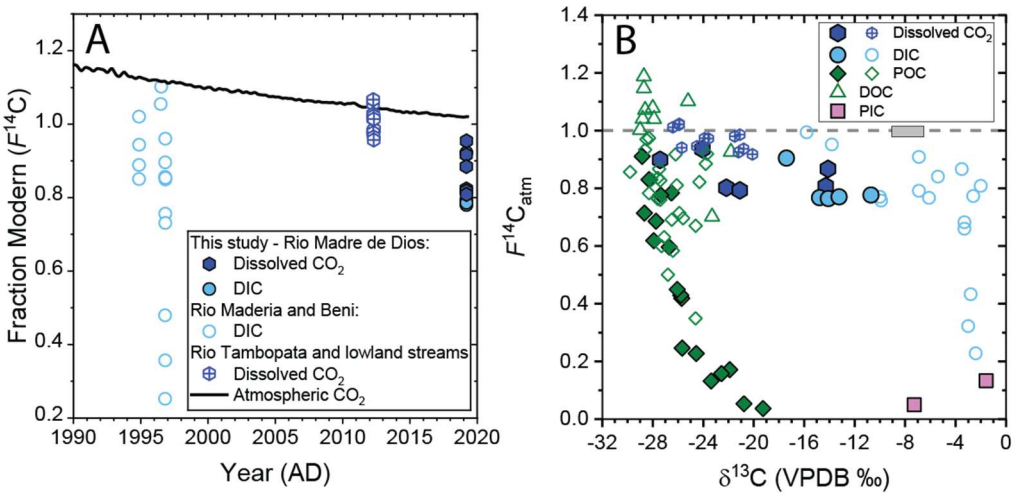

847

848 **Figure 2: Isotopic composition of DIC and CO_2 in the Madre de Dios Basin. A)** The
849 radiocarbon activity (reported as Fraction Modern, $F^{14}C$) of the dissolved CO_2 and DIC
850 measured in this study (filled symbols) alongside published data from the Rio Tambopata and
851 small lowland streams [47] and from the wider Maderia Basin and neighbouring Rio Beni [9]. The
852 atmospheric CO_2 value is shown by the black line [54]. **B)** The $F^{14}C$ values normalised to the
853 value of the atmosphere at time of sampling ($F^{14}C_{atm}$) for the river carbon pools against the
854 stable isotope composition ($\delta^{13}C$, ‰). Filled symbols are samples from the Madre de Dios
855 (Fig. 1) from this study, while open symbols are prior measurements of DIC, DOC and POC
856 [9]and dissolved CO_2 from close by sampling locations. Grey box indicates the range of
857 compositions for atmospheric CO_2 for reference.

858

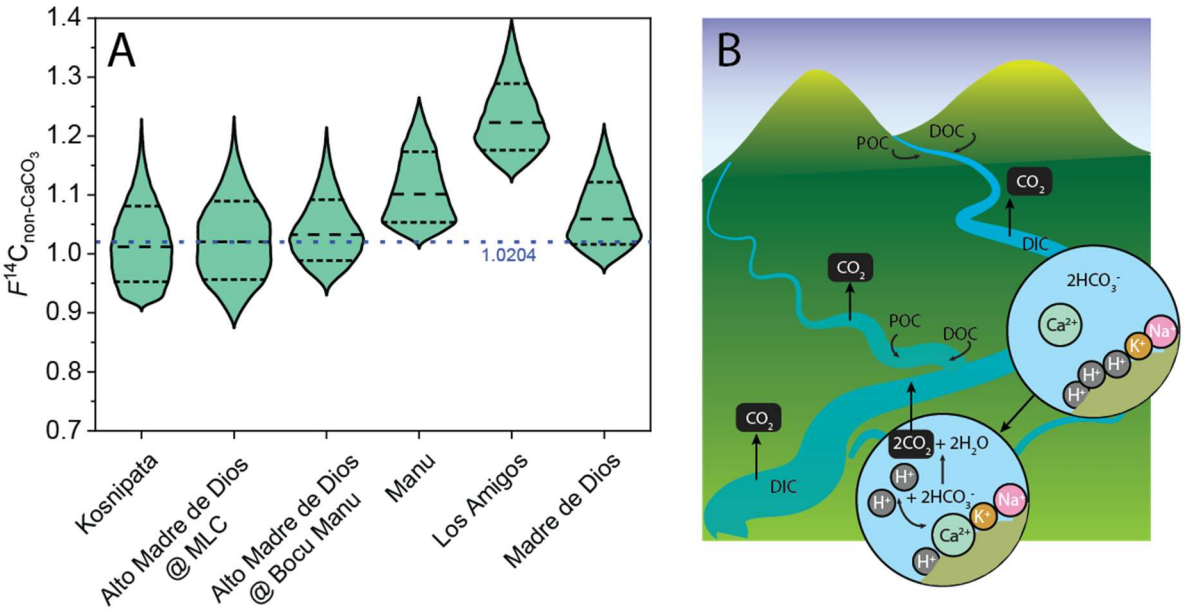

Figure 3: Source and drivers of river CO_2 release across this Andes to Amazon lowland transect. A. Modelled radiocarbon values ($F^{14}C$) of the non-calcium carbonate mineral derived DIC in the river load (Methods). Dashed lines show the medium and inter-quartile range of simulated values, with the distribution shown as a violin plot. The blue dashed line is the $F^{14}C$ value of the atmosphere at the time of sampling. Values below this line reflect inputs from aged carbon sources (likely soil or rock organic carbon respiration), while values above this line are from decadal-aged organic matter sources as discussed in the main text. **B.** Delivery and transport of POC, DOC and DIC in this system. Inset shows how cation exchange onto mineral or organic matter surfaces (brown edge) could drive CO_2 release in the wet season transect and act to reduce the DIC export.